RSC Advances

ROYAL SOCIETY OF CHEMISTRY

www.rsc.org/advances

RSC Advances

COMMUNICATION

Synthesis of heteroatom-carbon nanosheets by solution plasma processing using *N*-methyl-2-pyrrolidone as precursor

Received 00th January 20xx,
Accepted 00th January 20xx

DOI: 10.1039/x0xx00000x

www.rsc.org/

Koangyong Hyun,[a] Tomonaga Ueno,[ac] Oi Lun Li[ac] and Nagahiro Saito*[abcd]

Nitrogen-carbon nanosheets (NCNS), composed of multi-layer graphene with turbostratic stacking, were successfully synthesized through a solution plasma processing (SPP) at room temperature and an atmospheric pressure. The plasma was generated in 200 mL of *N*-methyl-2-pyrrolidone (NMP), which was applied as the carbon and nitrogen precursors. The NCNS presented an electrical resistivity of 0.065 Ω cm, which is comparable with that of N-doped carbon nanofibers (CNFs) and N-doped carbon nanotubes (CNTs). The synthesis rate of NCNS was 20 mg min^{-1}. From the characteristics analyses, NCNS showed the surface area of 277 m^2 g^{-1}, a pore volume of 0.95 cm^3 g^{-1} and a moderate nitrogen content of 1.3 at%. The synthesized NCNS also exhibited catalytic activity towards oxygen reduction reaction (ORR). This unique synthesis method can be applicable to synthesize multiple types of heteroatom-carbon nanosheets.

Introduction

Two-dimensional (2D) carbon nanosheets (CNS), which is composed of few- to multi-layer graphene,[1,2] are being extensively explored in many fields, such as in lithium-ion batteries,[3] supercapacitors (SCs),[4] organic solar cells,[5] sensitive gas-detection materials,[6] field emission (FE),[7] carbon dioxide (CO_2) adsorption,[8] and fuel cells,[9] Recently, CNS shows high popularity because of their many edges, chemical stability, high surface area and height-to-thickness ratio and their novel physical and chemical properties inherited from graphene.[1,2, 10]

Conventionally, CNS have been synthesized by the diverse chemical vapor deposition (CVD) of bottom-up synthesis methods, such as in microwave plasma-enhanced CVD,[11] hot-filament CVD,[12] direct-current (DC) discharge plasma CVD,[13] etc. However, these synthesis methods have complications. They inevitably require high processing temperatures and complicated instruments, impurities caused by metal catalyst, low production yield and high cost in operation.[14,15] In particular, only a few routes for the synthesis of CNS doped with heteroatom, which have been reported to tailor its electronic property and chemical reactivity,[16,17] have been reported. Yang *et al*.[18] reported that graphene doped with nitrogen and sulfur for oxygen reduction reaction can be obtained by high temperature thermal annealing. Shao *et al*.[19] obtained nitrogen-doped graphene by exposing graphene to nitrogen plasma. Wei *et al*. [20] produced the nitrogen-doped carbon nanosheets with combination method of hydrolysis and pyrolysis. Qu *et al*.[21] also reported the synthesis of nitrogen-doped graphene by CVD method with NH_3, for oxygen reduction reaction. They exhibited the enhanced physical and chemical properties for its electrochemical application. However, these methods consisted of multi-step treatments and required long treatment times.

Recently, solution plasma processing (SPP), a non-equilibrium liquid-phase plasma at atmospheric pressures,[22] has attracted a wide range of applications because of its versatility in nanoparticle synthesis,[23–25] the surface modification of metals,[26] water purification,[27] the depolymerization of natural biopolymers,[28] and the functionalization of multi-walled carbon nanotubes (CNTs).[29] In SPP, carbon materials can be synthesized through complex reactions; this includes C–H abstraction and C–C bonding as precursors in the non-thermal plasma discharge of organic solutions.[30–33]

In this study, we acknowledge the difficulties of conventional methods and applied SPP to synthesize heteroatom-doped CNS as bottom-up synthesis method for the first time. The nitrogen-carbon nanosheets (NCNS), composed of multi-layer graphene with turbostratic stacking, were successfully synthesized with SPP using *N*-methyl-2-pyrrolidone (NMP) as a simple single-source precursor at room temperature and an atmospheric pressure. Compared with conventional methods, SPP has several advantages, such as a

[a] Department of Materials, Physics and Energy Engineering, Graduate School of Engineering, Nagoya University, Nagoya 464-8603, Japan.
[b] Social Innovation Design Center (SIDC), Institute of Innovation for Future Society, Nagoya University, Nagoya 464-8603, Japan.
[c] Green Mobility Collaborative Research Center, Nagoya University, Nagoya 464-8603, Japan.
[d] Core Research for Evolutional Science and Technology (CREST), Japan Science and Technology Agency (JST), Kawaguchi, Saitama 332-0012, Japan.
E-mail: hiro@rd.numse.nagoya-u.ac.jp

high yield, a short synthesis time, a simple experimental apparatus, no impurity issues and the ability to operate at room temperature. The synthesis rate of NCNS was found to be about 20 mg min^{-1}, which was about 285 times greater than that of conventional CVD methods (0.07 mg min^{-1}).[34] These advantages have facilitated the potential extension of SPP to material processing for industrial applications. Furthermore, nitrogen atoms within carbon matrix have been reported to improve the electrocatalytic performance of carbon electrode materials.[32,35,36] In this study, electrochemical analysis was also conducted for the synthesized NCNS and the result demonstrated that the NCNS could be applicable as an electrocatalyst for ORR. This study shed light on a new strategy for the feasible synthesis of NCNS for use as cathode catalysts in a fuel cell application.

Experimental methods

Synthesis of nitrogen-carbon nanosheets (NCNS) by solution plasma processing (SPP)

Fig. 1 illustrates a schematic illustration of the solution plasma system for the synthesis of NCNS. The discharge was generated at the gap between a pair of tungsten electrode (1 mm in diameter, 99.9% purity, Nilaco) that were placed at the center of a glass reactor. A gap distance between two electrodes was fixed at 1.5 mm. A bipolar high voltage pulse of 2.0 kV was applied to the tungsten electrodes using a bipolar pulsed power supply (Kurita, Japan) with a repetition frequency of 25–200 kHz and a pulse width of 1.0 μs. An organic solution, *N*-methyl-2-pyrrolidone (NMP) (C_5H_9NO 99.0%, Kanto Chemical), was used as the precursor of NCNS. High-repetition frequency discharges were generated and maintained in 200 mL of the chemicals under vigorous stirring for 5 min. After the synthesis, the black powder was separated by vacuum filtration through a polytetrafluoroethylene (PTFE) membrane filter with a pore size of 100 nm. The synthesized NCNS were then dried in oven at 200 °C for 1 h. We could then get the black powder of 100 ± 4 mg after the process was completed. This synthetic method showed reproducibility through 5 times preparation. In this study, NCNS was achieved only at a high frequency of 200 kHz, whereas NCNS could not be formed at low frequency region (25 and 100 kHz), as shown in Fig. S1† and S2†. Therefore, the NCNS synthesized at 200 kHz was selected to investigate throughout this study.

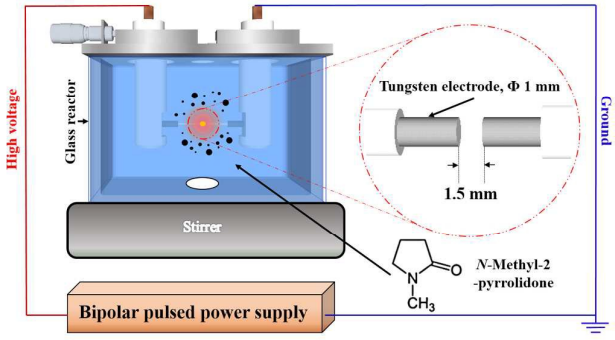

Fig. 1 Schematic diagram of solution plasma processing (SPP).

Characterization

The morphology of the synthesized NCNS was investigated by transmission electron microscopy (TEM, JEM-2500SE; JEOL) with an accelerating voltage of 200 kV. The X-ray diffraction (XRD) patterns of the products were recorded on Rigaku Smartlab with Cu Kα radiation (λ = 0.154 nm). Raman spectra were collected using Raman spectroscopy (NRS-100, JASCO) with an excitation laser wavelength of 532.5 nm. The surface area, pore volume and average pore size of the synthesized sample were measured with a Belsorp mini-II analyzer at liquid nitrogen temperature (77 K), following the Brunauer-Emmett-Teller (BET) theory. X-ray photoelectron spectroscopy (XPS, PHI 5000 VersaProbe II; ULVAC-PHI) measurements were performed using an Mg Kα X-ray sources. Elemental analysis of C, H and N was performed using an elemental analyzer (Perkin Elmer 2400 Series).

Electrical resistivity test

The electrical resistivity was measured with a device consisting of two probes: resistivity meter (2001 multimeter, TFF Corp., Keithley Instruments) and DC constant power supply (model 692A, Metronix Corp.). Each sample was inserted in a hollow Teflon cylinder (inner diameter: 0.5 cm). They were then compressed to 0.6 MPa in air between the two brass pistons of the electrodes. The electrical resistivity was measured while the samples were being pressed.[37–39]

Electrochemical measurements

Electrochemical analysis of NCNS was carried out with a conventional three-electrode cell system (Hokuto Denko Inc. HZ5000) using a glassy carbon (GC) disk (diameter: 3 mm) as the working electrode, a platinum wire as the counter electrode and Ag/AgCl in saturated KCl as the reference electrode. Then, 5.0 mg of NCNS was dispersed in 500 μL of ethanol and 20 μL of Nafion (5 wt%, Aldrich). The mixture for catalyst ink was ultrasonicated until a homogeneous suspension was formed. For preparing the working electrode, the suspension was dropped on the GC electrode and dried at room temperature. The cyclic voltammetry (CV) was measured in 0.1 M KOH (Kanto Chemical) and saturated in O_2 and N_2 with a scan rate of 50 mV s^{-1}. The linear sweep voltammetry (LSV) was conducted in O_2-saturated 0.1 M KOH with a scan rate of 10 mV s^{-1} at 1600 rpm using a rotating disk electrode (RDE). The durability of NCNS was perfromed by the measurement of current–time chrono-amperometric response at a constant potential of –0.4 V in O_2-saturated 0.1M KOH solution for 20 000 s at a rotating speed of 1600 rpm. The tolerance to the methanol crossover effect was also evaluated.

Results and discussion

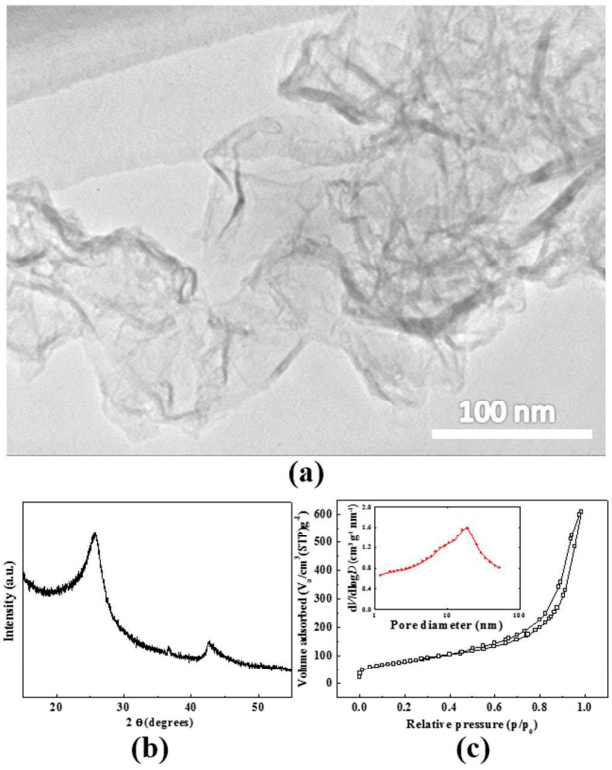

Fig. 2 (a) Transmission electron microscopy (TEM) images of nitrogen-carbon nanosheets (NCNS), (b) X-ray diffraction (XRD) patterns and (c) N_2 adsorption-desorption plots with inset showing pore diameter distribution curves of NCNS.

The morphology and structure of NCNS was investigated using TEM. Fig. 2a reveals the wrinkled 2D nanosheet-like morphology of the as-synthesized NCNS on a carbon TEM grid. Multiple TEM images were observed from various locations of the NCNS sample and other nanostructures were not discovered. Fig. 2b shows a typical powder XRD pattern of the as-synthesized NCNS. The NCNS exhibited two sharp peaks, a characteristic of a disordered turbostratic phase, at around 2θ of 25.8° and 43.1°, corresponding to the (002) and (100/101) graphite planes, respectively.[40] The interlayer spacing was calculated to be approximately 0.346 nm from the position of the (002) diffraction peak, which is slightly larger than that of bulk graphite (0.335 nm). The larger interlayer distance can be ascribed to turbostratic disorder.[37] Fig. 2c displays the N_2 adsorption–desorption isotherm of NCNS. The specific surface area and pore structure properties were determined by using BET theory. The N_2 adsorption isotherm curve of NCNS showed a typical IV profile with an H1 hysteresis loop, in accordance with the International Union of Pure and Applied Chemistry's (IUPAC's) classification.[41] The NCNS possesses a total pore volume of 0.95 $cm^3 g^{-1}$, a mean pore size of 14 nm and a BET surface area of 277 $m^2 g^{-1}$. Moreover, using the Barrett–Joyner–Halenda (BJH) method, the pore size distribution plot revealed a sharp peak at 18.9 nm, as shown in the inset of Fig. 2c. Thus, NCNS contained highly mesoporous structures. It is

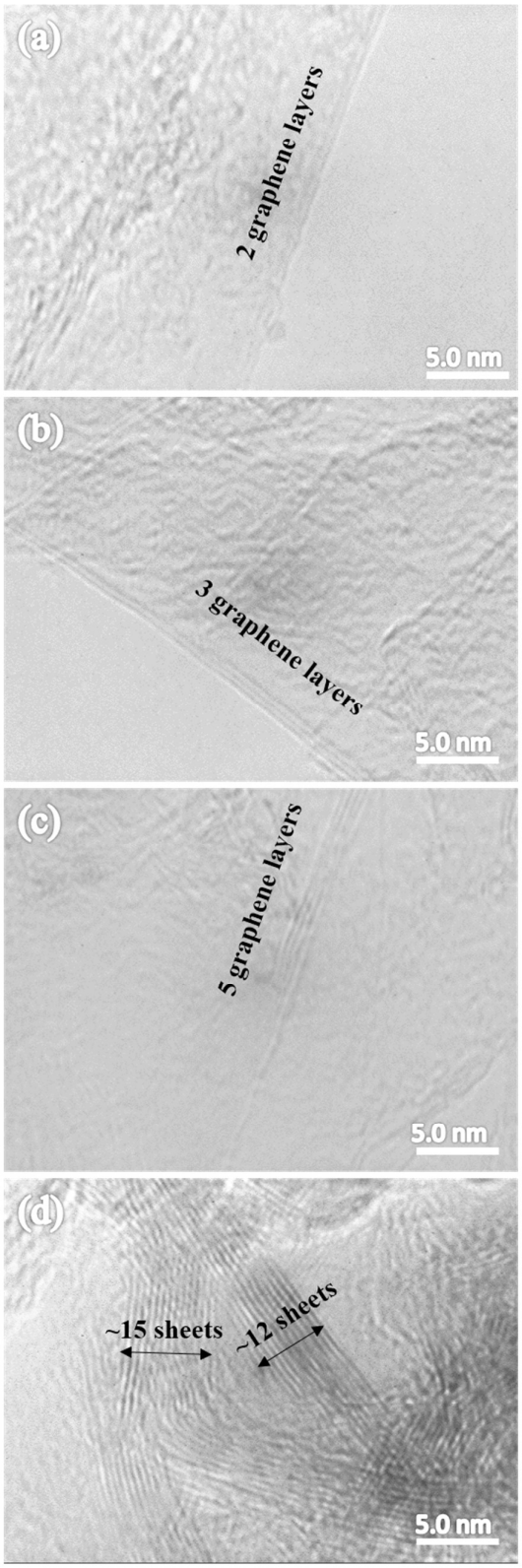

Fig.3 High-magnification transmission electron microscopy images of nitrogen-carbon nanosheets (NCNS) with (a) two graphene layers, (b) three graphene layers, (c) five graphene layers and (d) multiple graphene layers.

suspected that each carbon sheet would agglomerate due to their small grain size, which causes a relatively low surface area. Consequently, it is possible that mesoporous structures are formed by the space between agglomerated carbon nanosheets.

High-magnification TEM images in Fig. 3a–d display the graphene layer number within NCNS. Fig. 3a reveals a single nanosheet consisting of two parallel fringes. The fringes were defined as the cross section of the planar nanosheet's folded edge, indicating two atom-thick layer sheets. Three to five graphene layers were also observed, as displayed in Fig. 3b and 3c. However, the morphology of NCNS was mainly composed of multi-layered graphene, as indicated in Fig. 3(d).

Fig. 4a shows the Raman spectrum of NCNS, of which containing three main features of D, G and 2D-bands. The D-band represents the disorder-induced band at 1338 cm^{-1} that depends on the presence of structural defects and disorder in the lattice.[42,43] The G-band at 1575 cm^{-1} is attributed to the vibrations of the in-plane sp^2 phonon of carbon atoms in a 2D hexagonal lattice.[44,45] The intensity ratio of the D-band and G-band (I_D/I_G) is typically related to the disorder degree, the degree of graphitization and the in-plane crystalline size L_a.[42,43,46] The intensity ratio of I_D/I_G was about 0.6, suggesting that the carbon nanosheets are long-range ordered graphitized carbon.[47] The crystalline size L_a of NCNS was calculated by an equation which is given by

$$L_a = (2.4 \times 10^{-10})\lambda_l^4 (I_D/I_G)^{-1}, \quad (1)$$

where λ_l is the laser line wavelength in nm.[46] The laser line was shown to be 32.2 nm of the crystalline size. The 2D-band at 2675 cm^{-1} is associated to the second-order of the D-band. Furthermore, the position and intensity of the 2D-band, which is a characteristic peak in the higher-order carbon structure, can be employed to identify the number of layers in graphene-related materials.[48] The full width at half maximum (FWHM) of the 2D peak was approximately 70 cm^{-1} and the single Lorentzian line shape of the 2D peak, as shown in Fig. 4b, looks similar to monolayer graphene. These results suggest that NCNS should be constructed by multi-layer graphene with turbostratic stacking.[49–51]

As shown in Fig. 5a, the XPS survey spectra of NCNS show a narrow C 1s peak at 284.5 eV, a weak O 1s peak at 532.5 eV and a much weaker N 1s peak at 399.5 eV. XPS measurement provided the surface elemental composition of NCNS. The contents of C, N and O elements were 96.2, 1.3 and 2.5 at%, as shown in Table 1. From the elemental analysis (EA) results, the carbon, nitrogen and hydrogen content in the NCNS were 92.3, 1.3 and 0.7 wt%, which were similar with that of the XPS measurement. It can be assumed that the nitrogen atoms existed in NCNS, homogeneously. The high-resolution C 1s peak of the NCNS revealed the one main peak at 284.5 eV (C-1) corresponding to sp^2 hybridized graphitic carbon, as shown in Fig 5b, which indicated that NCNS was mostly composed of a conjugated honeycomb lattice. And small signals at 285.6 (C-2) and 286.5 eV (C-3) could be assigned to C–O/C=N and C–N/C=O species, respectively.[52] Fig. 5c shows the high-resolution N 1s peak which was composed with several types of N coordination such as pyridinic N (N-1, 398.5 eV), pyrrolic

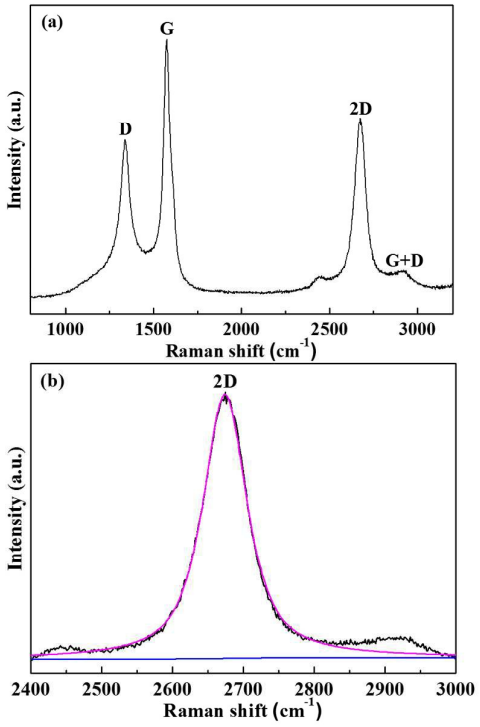

Fig. 4 (a) Raman spectroscopy of nitrogen-carbon nanosheets (NCNS) obtained with laser at 532.5 nm and (b) two-dimensional (2D) peaks in Raman spectrum fitted by a single Lorentzian function.

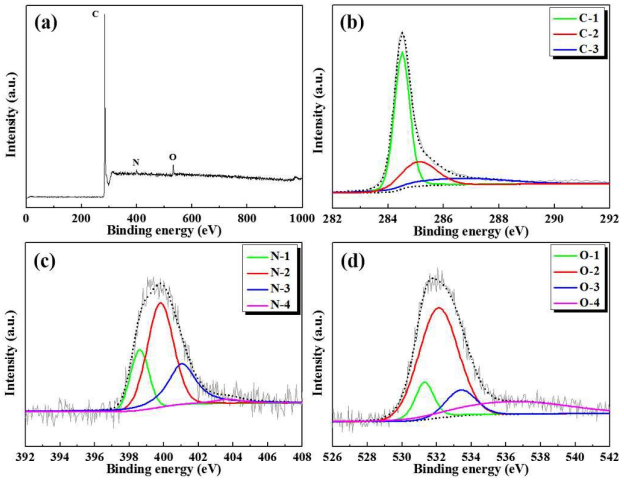

Fig. 5 Survey X-ray photoelectron spectroscopy (XPS) spectra (a); C 1s spectra of NCNS (b); N 1s spectra of NCNS (c) ; O 1s spectra of NCNS (d).

Table 1 Summary of surface and bulk elemental compositions of NCNS.

	C	N	O	H
Surface elemental composition XPS (at%)	96.2	1.3	2.5	-
Bulk elemental composition EA (wt%)	92.3	1.3	-	0.7

Table 2 Electrical resistivity and nitrogen content of NCNS compared to nitrogen-doped carbon nanofibers (CNFs) and carbon nanotubes (CNTs) as references.

Carbon material	Nitrogen	(Ω·cm) at ambient temperature	Ref.
Nitrogen-doped CNFs	3.1 wt%	0.065	(56)
Nitrogen-doped CNTs	0.32 at%	~ 0.04	(57)
NCNS	1.3 at%	0.065	Present work

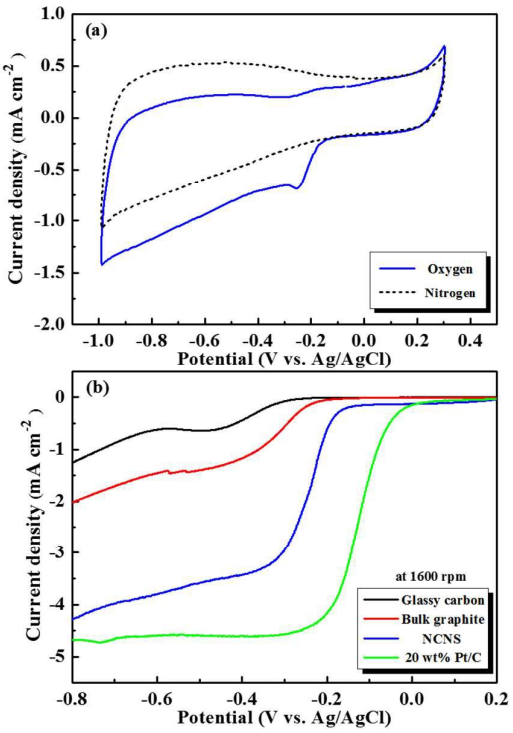

Fig. 6 (a) Cyclic voltammetry (CV) and (b) linear sweep voltammetry (LSV) of nitrogen-carbon nanosheets (NCNS) in 0.1 M KOH electrolyte at scan rate of 50 mV s^{-1} and 10 mV s^{-1}, respectively.

N (N-2, 400 eV), graphitic N (N-3, 401.2 eV) and oxidized N (N-4, 403.7 eV).[30,53] The content of N coordination type revealed 28.9, 49.8, 19.4 and 1.9 %, corresponding to pyridinic N, pyrrolic N, graphitic N and oxidized N, respectively. Among the type, the pyridinic N and graphitic N play a leading part in the oxygen reduction reaction.[54] The 48.3 % of nitrogen atoms in NCNS are anticipated to appear the positive effects for electrocatalytic activity. Fig. 5d shows the high-resolution O 1s peak which was composed with several types of O coordination such as O-1 (C=O, 531.3 eV), O-2 (C–O, 532.1 eV), O-3 (O–C=O, 533.4 eV), O-4 (adsorbed oxygen or water, 536.4 eV).[55]

Table 2 shows the electrical resistivity of NCNS compared to that of carbon nanofibers (CNFs) and carbon nanotubes (CNTs) for reference. The resistivity was 0.065 and 0.04 Ωcm

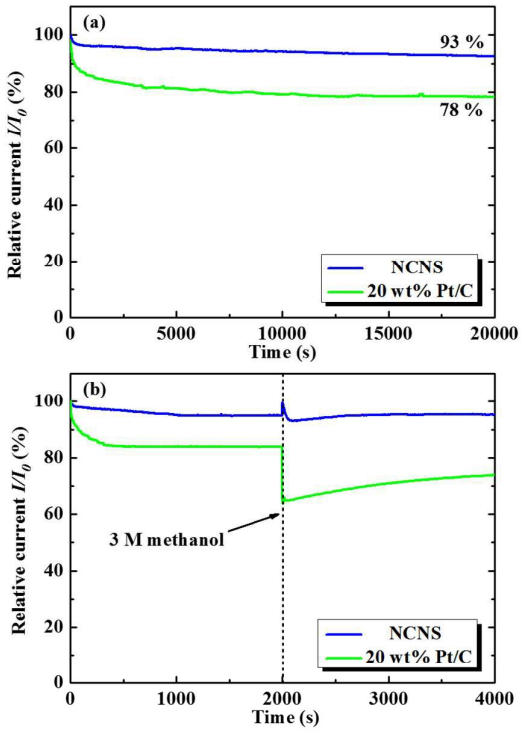

Fig. 7 (a) Durability evaluation of NCNS and 20 wt% Pt/C with current–time chronoamperometric response at a constant potential of –0.4 V in O_2-saturated 0.1 M KOH solution for 20 000 s at a rotating speed of 1600 rpm. (b) Chronoamperometric response (1600 rpm) with the introduction of 3 M methanol at 2000 s. The arrow indicated the injection of 3 M methanol.

corresponding to the nitrogen-doped CNFs and CNTs, respectively.[56,57] The resistivity of the NCNS was 0.065 Ω cm and was in the same order of magnitude compared to that of CNFs and CNTs. We believe that the nanosheet structural feature of the multi-layer graphene, which has a high electron mobility with abundant π conjugation system, was the main reason of low resistivity.[58] Also, the high crystallinity and few defect of the physically bonded networks, as shown in Raman spectroscopy, could be assumed it as the one of the reason.[59]

Fig. 6a shows the CV curve of NCNS. It was measured in an aqueous 0.1 M KOH electrolyte under O_2 and N_2 saturated condition in the potential range of –1.0 to 0.3 V and a scan rate of 50 mV s^{-1}. No obvious redox peaks appeared under N_2-saturated 0.1 M KOH electrolyte. In contrast, the CV curve under O_2-saturated 0.1 M KOH electrolyte revealed a prominent and well-defined cathodic peak at −0.25 V, corresponding to the occurrence of oxygen reduction reaction (ORR) of the electrodes in O_2 ambience. The onset potential was observed at −0.17 V. In the results of LSV, shown in Fig. 6b, the ORR activity of the NCNS revealed a significantly higher onset potential than that of bulk graphite. It can be assumed that the existence of nitrogen within the carbon matrix provided a superior electrocatalytic activity.[60] However, the ORR activity of NCNS was still much inferior to that of the commercial 20 wt% Pt on Vulcan XC-72. The ORR activity in

terms of onset potential of NCNS in our study was compared with that of N-doped graphene reported in several previous works (see Table S1†).[61–63] It was found that the ORR activity of NCNS was much inferior to N-doped graphene. The weak ORR activity of NCNS may possibly be due to a relatively low N doping content, especially pyridinic N and graphitic N bonding states. It has been known that pyridinic N and graphitic N species are the important factors in significantly enhancing ORR activity, whereas pyrrolic N had a little effect on the ORR activity. The synthesis of NCNS with controllable N bonding sates (*i.e.*, high content of pyridinic N and graphitic N) are still underway in our laboratory.

As shown in Fig. 7a, the relative current (I/I_0) of NCNS revealed a slow attenuation than that of commercial 20 wt% Pt/C. After 20 000s, the high I/I_0 of NCNS was maintained with approximately 93 %, whereas the Pt/C exhibited the low I/I_0 of 78 %. Furthermore, in the tolerance to the methanol crossover effect, the NCNS was quite stable as shown in Fig. 7b, which 3 M methanol was injected into O_2-saturated 0.1 M KOH solution during the measurement of the chronoamperometric response at a rotation rate of 1600 rpm for 2000 s. On the other hand, the 20 wt% Pt/C showed the sharp decrease of the I/I_0 after the addition of methanol. These results presented that the NCNS had the better electrochemical stability and excellent methanol tolerance than that of the 20 wt% Pt/C.

Conclusions

We have successfully synthesized NCNS through a specific type of plasma discharge in liquid, named solution plasma processing (SPP), under room temperature and atmospheric pressure. The organic solution, *N*-methyl-2-pyrrolidone (NMP), was applied as a single precursor where nitrogen atoms were simultaneously embedded within the carbon matrix through one-pot synthesis. From elemental analysis, the carbon, hydrogen and nitrogen contents were, respectively, 92.3, 0.7 and 1.3 wt%. Detailed investigations of the properties of NCNS revealed that the samples consisted of multi-layer graphene with turbostratic stacking. NCNS demonstrated a low resistivity of 0.065 Ω cm, of which is in the same order of magnitude of N-doped CNFs and N-doped CNTs. The surface area and pore volume of NCNS were 277 m^2g^{-1} and 0.95 cm^3g^{-1}, respectively, which indicated the material were mesoporous structures and composed of agglomerated nanosheets. Although NCNS exhibited an insufficiently low catalytic activity toward ORR, its stability and methanol tolerance were better than those of 20 wt% Pt/C. This demonstrates the capability as an ORR electrocatalyst. Therefore, this study may offer a new strategy for the feasible synthesis of CNS in the fuel cell application.

Acknowledgments

This research was financially supported by Core Research for Evolutional Science and Technology (CREST) of Japan Science and Technology Agency (JST).

Notes and references

1 Z. Wang, H. Ogata, S. Morimoto, M. Fujishige, K. Takeuchi, Y. Hashimoto and M. Endo, *Carbon*, 2014, **72**, 421.
2 Z. Wang, H. Ogata, S. Morimoto, M. Fujishige, K. Takeuchi, Y. Hashimoto and M. Endo, *Carbon*, 2014, **68**, 360.
3 L. Chen, Z. Wang, C. He, N. Zhao, C. Shi, E. Liu and J. Li, *ACS Appl. Mater. Interfaces*, 2013, **5**, 9537.
4 H. Wang, Z. Xu, A. Kohandehghan, Z. Li, K. Cui, X. Tan, T. J. Stephenson, C. K. Kingondu, C. M. B. Holt, B. C. Olsen, J. K. Tak, D. Harfield, A. O. Anyia and D. Mitlin, *ACS Nano*, 2013, **7**, 5131.
5 S. Y. Son, J. M. Yun, Y. J. Noh, S. Lee, H. N. Jo, S. I. Na, H. I. Joh, *Carbon*, 2015, **81**, 546.
6 J. J. Wang, M. Y. Zhu, R. A. Outlaw, X. Zhao, D. M. Manos and B. C. Holloway, *Appl. Phys. Lett.*, 2004, **85**, 1265.
7 M. Y. Zhu, R. A. Outlaw, M. Bagge-Hansen, H. J. Chen and D. M. Manos, *Carbon*, 2011, **49**, 2526.
8 G. P. Hao, Z. Y. Jin, Q. Sun, X. Q. Zhang, J. T. Zhang and A. H. Lu, *Energy Environ. Sci.*, 2013, **6**, 3740.
9 C. Z. Li, Z. B. Wang, X. L. Sui, L. M. Zhang and D. M. Gu, *Carbon*, 2015, **93**, 105.
10 W. Liu, T. Dang, Z. Xiao, X. Li, C. Zhu and X. Wang, *Carbon*, 2011, **49**, 884.
11 Z. Wang, M. Shoji, H. Ogata, *Appl. Surf. Sci.*, 2011, **257**, 9082.
12 N. G. Shang, F. C. K. Au, X. M. Meng, C. S. Lee, I. Bello and S. T. Lee, *Chem. Phys. Lett.*, 2002, **358**, 187.
13 A. N. Obraztsov, A. A. Zolotukhin, A. O. Ustinov, A. P. Volkov, Y. Svirko and K. Jefimovs, *Diamond Relat. Mater.*, 2003, **12**, 917.
14 Q. Kuang, S. Y. Xie, Z. Y. Jiang, X. H. Zhang, Z. X. Xie, R. B. Huang and L. S. Zheng, *Carbon*, 2004, **42**, 1737.
15 W. Wang, S. Chakrabarti, Z. Chen, Z. Yan, M. O. Tade, J. Zou and Q. Li, *J. Mater. Chem. A*, 2014, **2**, 2390.
16 E. C. Anota, H. H. Cocoletzi and M. Castro, *J. Comput. Theor. Nanosci.*, 2013, **10**, 1
17 M. K. Rybarczyk, M. Lieder and M. Jablonska, *RSC Adv.*, 2015, **5**, 44969
18 S. Yang, L. Zhi , K. Tang , X. Feng , J. Maier and K. Müllen, *Adv. Funct. Mater.*, 2012, **22**, 3634.
19 Y. Shao, S. Zhang, M. H. Engelhard, G. Li, G. Shao, Y. Wang, J. Liu, I. A. Aksay and Y. Lin, *J. Mater. Chem.*, 2010, **20**, 7491.
20 W. Wei, H. Liang, K. Parvez, X. Zhuang, X. Feng and K. Mullen, *Angew. Chem. Int. Ed.*, 2014, **126**, 1596.
21 L. Qu, Y. Liu, J. B. Baek and L. Dai, *ACS Nano*, 2010, **4**, 1321
22 O. Takai, *Pure Appl. Chem.*, 2008, **80**, 2003.
23 T. Shirafuji, J. Ueda, A. Nakamura, S. P. Cho, N. Saito and O. Takai, *Jpn. J. Appl. Phys.*, 2013, **52**, 126202.
24 A. Watthanaphanit, G. Panomsuwanc and N. Saito, *RSC Adv.*, 2014, **4**, 1622.
25 G. Panomsuwan, A. Watthanaphanit, T. Ishizaki and N. Saito, *Phys. Chem. Chem. Phys.*, 2015, **17**, 13794.
26 V. Anita, N. Saito and O. Takai, *Thin Solid Films*, 2006, **506–507**, 364.
27 B. R. Locke, M. Sato, P. Sunka, M. R. Hoffmann and J. S. Chang, *Ind. Eng. Chem. Res.*, 2006, **45**, 882.
28 A. Watthanaphanit and N. Saito, *Polym. Degrad. Stab.*, 2013, **98**, 1072.
29 T. Shirafuji, Y. Noguchi, T. Yamamoto, J. Hieda, N. Saito, O. Takai, A. Tsuchimoto, K. Nojima and Y. Okabe, *Jpn. J. Appl. Phys.*, 2013, **52**, 125101.
30 G. Panomsuwan, S. Chiba, Y. Kaneko, N. Saito and T. Ishizaki, *J. Mater. Chem. A*, 2014, **2**, 18677.
31 O. L. Li, J. Kang, K. Urashima and N. Saito, *Int. J. Environ. Sci*. Technol., 2013, **7**, 31.
32 D. W. Kim, O. L. Li and N. Saito, *Phys. Chem. Chem. Phys.*, 2015, **17**, 407.
33 J. Kang, O. L. Li and N. Saito, *Nanoscale*, 2013, 5, 6874.

34 T. Hagino, H. Kondo, K. Ishikawa, H. Kano, M. Sekine and M. Hori, *Appl. Phys. Exp.*, 2012, **5**, 035101.
35 G. Panomsuwan, N. Saito and T. Ishizaki, *Phys. Chem. Chem. Phys.*, 2015, **17**, 6227.
36 Y. Jiao, Y. Zheng, M. Jaroniec and S. Z. Qiao, *J. Am. Chem. Soc.*, 2014, **136**, 4394.
37 J. S. Gonzalez, A. M. Garcıa, M. F. A. Franco and V. G. Serrano, *Carbon*, 2005, **43**, 741.
38 A. Celzard, J. F. Mareche, F. Payot and G. Furdin, *Carbon*, 2002, **40**, 2801.
39 B. Marinho, M. Ghislandi, E. Tkalya, C. E. Koning and G. D. With, *Powder Technology*, 2012, **221**, 351.
40 D. Bhattacharjya, H. Y. Park, M. S Kim, H. S. Choi, S. N. Inamdar and J. S. Yu, *Langmuir*, 2014, **30**, 318.
41 Z. A. ALOthman, *Materials*, 2012, **5**, 2874.
42 A. C. Ferrari and J. Robertson, *Phys. Rev. B Condens. Matter Mater. Phys.*, 2000, **61**, 14095.
43 A. C. Ferrari and J. Robertson, *Phys. Rev. B Condens. Matter Mater. Phys.*, 2001, **64**, 075414
44 J. W. Liu, M. W. Shao, X. Y. Chen, W. C. Yu, X. M. Liu and Y. T. Qian, *J. Am. Chem. Soc.*, 2003, **125**, 8088.
45 J. W. Liu, M. W. Shao, Q. Tang, S. Y. Zhang and Y. T. Qian, *J. Phys. Chem. B*, 2003, **107**, 6329.
46 L. G. Cancado, K. Takai. T. Enoki, M. Endo, Y. A. Kim, H. Mizusaki, A. Jorio, L. N. Coelho, R. Magalhães-Paniago and M. A. Pimenta, *Appl. Phys. Lett.*, 2006, **88**, 163106.
47 Q. Kuang, S. Y. Xie, Z. Y. Jiang, X. H. Zhang, Z. X. Xie, R. B. Huang and L. S. Zheng, *Carbon*, 2004, **42**, 1737.
48 Z. Wang, M. Shoji, K. Baba, T. Ito, H. Ogata, *Carbon*, 2014, **67**, 326.
49 P. R. Kidambi, C. Ducati, B. Dlubak, D. Gardiner, R. S. Weatherup, M. B. Martin, P. Seneor, H. Coles and S. Hofmann, *J. Phys. Chem. C*, 2012, **116**, 22492.
50 L. M. Malard, M. A. Pimenta, G. Dresselhaus and M. S. Dresselhaus, *Phys. Rep.*, 2009, **473**, 51.
51 Z. Wang, H. Ogata, S. Morimoto, M. Fujishige, K. Takeuchi, H. Muramatsu, T Hayashi, J. Ortiz-Medina, M. Z. M. Yusop, M. Tanemura, M. Terrones, Y. Hashimoto and M. Endo, *J. Mater. Chem. A*, 2015, **3**, 14545.
52 Q. Liu, Y. Duan, Q. Zhao, F. Pan, B. Zhang and J. Zhang, Langmuir 2014, **30**, 8238.
53 Y. H. Lee, Y. F. Lee, K. H. Chang and C. C. Hu, Electrochem. Commun., 2011, **13**, 50.
54 L. Lai, J. R. Potts, D. Zhan, L. Wang, C. K. Poh, C. Tang and H. Gong, *Energy Environ. Sci*., 2012, **5**, 7936.
55 R. Singhal and V. Kalra, *J. Mater. Chem. A*, 2015, **3**, 377.
56 Z. R. Ismagilov, A. E. Shalagina, O. Yu. Podyacheva, A. V. Ischenko, L. S. Kibis, A. I. Boronin, Y. A. Chesalov, D. I. Kochubey, A. I. Romanenko, O. B. Anikeeva, T. I. Buryakov and E. N. Tkachev, *Carbon*, 2009, **47**, 1922.
57 K. Fujisawa, T. Tojo, H. Muramatsu, A. L. Elias, S. M. Vega-Diaz, F. Tristan-Lopez, J. H. Kim, T. Hayashi, Y. A. Kim, M. Endo and M. Terrones, *Nanoscale*, 2011, **3**, 4359.
58 M. J. Allen, V. C. Tung and R. B. Kaner, *Chem. Rev.*, 2010, **110**, 132.
59 K. Hyun, T. Ueno and N. Saito, *Jpn. J. Appl. Phys.*, 2016, **55**, 01AE18.
60 D. W. Kim, O. L. Li, P. Pootawang and N. Saito, *RSC Adv.*, 2014, **4**, 16813.
61 J. L. Shi, G. L. Tian, Q. Zhang, M. Q. Zhao and F. Wei, *Carbon*, 2015, **93**, 702.
62 Z. Xu, H. Li, B. Yin, Y. Shu, X. Zhao, D. Zhang, L. zhang, K. Li, X. Houd and J. Lua, *RSC Adv.*, 2013, **3**, 9344.
63 D. W. Chang, H. J. Choi and J. B. Baek, *J. Mater. Chem. A*, 2015, **3**, 7659.

Synthesis of heteroatom-carbon nanosheets by solution plasma processing using *N*-methyl-2-pyrrolidone as precursor

Koangyong Hyun, [1] Tomonaga Ueno,[1,3] Oi Lun Li[1,3] and Nagahiro Saito[1,2,3,4]*

[1]*Department of Materials, Physics and Energy Engineering, Graduate School of Engineering, Nagoya University, Furo-cho, Chikusa-ku, Nagoya 464-8603, Japan*

[2]*Social Innovation Design Center (SIDC), Institute of Innovation for Future Society, Nagoya University, Furo-cho, Chikusa-ku, Nagoya 464-8603, Japan*

[3]*Green Mobility Collaborative Research Center, Nagoya University, Chikusa-ku, Nagoya 464-8603, Japan*

[4]*Core Research for Evolutional Science and Technology (CREST), Japan Science and Technology Agency (JST), Saitama 332-0012, Japan*

E-mail: hiro@rd.numse.nagoya-u.ac.jp

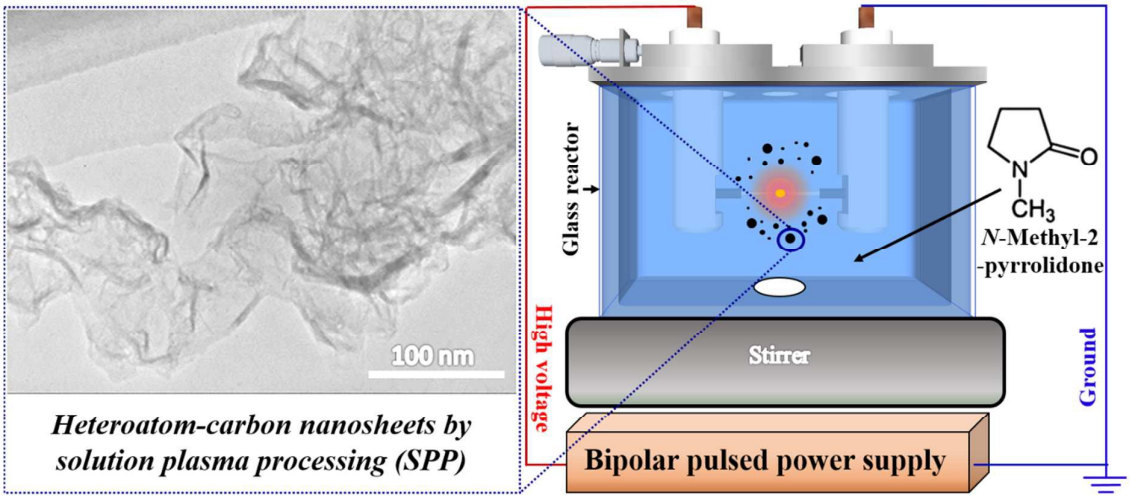

Heteroatom-carbon nanosheets, composed of multi-layer graphene with turbostratic stacking, were successfully synthesized through a solution plasma processing (SPP) with *N*-methyl-2-pyrrolidone at room temperature and an atmospheric pressure.